Analytical and Bioanalytical Chemistry (2020) 412:3871–3880
https://doi.org/10.1007/s00216-020-02607-7

RESEARCH PAPER

Electrochemical attack and corrosion of platinum electrodes in dielectrophoretic diagnostic devices

Daniel P. Heineck[1] · Benjamin Sarno[2] · Sejung Kim[2] · Michael Heller[1,2]

Received: 21 December 2019 / Revised: 28 February 2020 / Accepted: 18 March 2020 / Published online: 10 April 2020

Abstract

Though the advances in microelectronic device fabrication have realized new capabilities in integrated analytical and diagnostic platforms, there are still notable limitations in point-of-care sample preparation. AC electrokinetic devices, especially those leveraging dielectrophoresis (DEP), have shown potential to solve these limitations and allow for sample-to-answer in a single point-of-care device. However, when working directly with whole blood or other high conductance (~ 1 S/m) biological fluids, the aggressive electrochemical conditions created by the electrode can fundamentally limit the device operation. In this study, platinum wire-based electrode devices spanning circular polytetrafluorethylene (PTFE) wells and a planar microarray device with sputtered platinum electrodes were tested in plasma and PBS buffers of differing concentration across a wide range of frequencies and electric field intensities (AC voltages) to determine their respective safe regions of operation and to gain an understanding about the failure mechanisms of this class of device. At frequencies of 10 kHz and below, the upper bound of operation is the degradation of electrodes due to electrochemical attack by chlorine overcoming the native platinum oxide passivation. At higher frequencies, 100 kHz and above, the dielectric loss and subsequent heating of the buffer will boil before the electrodes suffer observable damage, due to the slow irreversible reaction kinetics. Effective dielectrophoretic capture of small biological particles at these frequencies is limited, and heat/oxidative denaturation of target material are a major concern. A new class of smaller devices, ones capable of high throughput at voltages low enough to maintain the integrity of the platinum passivation layer, is needed to mitigate these fundamental limitations.

Keywords Dielectrophoresis · Electrokinetics · Corrosion · Electrochemistry · Liquid biopsy · Point-of-care

Introduction

The design of point-of-care (POC) analytical and diagnostic workflows presents numerous challenges and integration of disparate processes. This said, the demand for these technologies is growing, as elegant and direct sample-to-answer processing methods can free up trained laboratory staff, save time and cost, reduce sample volume demands per test, and militate against sample degradation, bias, and error [1]. The past decade has seen a number of advances towards miniaturization and automation of analytical/diagnostic processes but still major issues exist in developing viable (POC) devices [2]. Most efforts for advancement have been focused on improvement and optimization of long, multi-step protocols that demand complex laboratory facilities and trained operators [3]. Working directly from undiluted patient blood or other patient fluid with minimal-to-zero sample preparation is an essential requirement for point-of-care diagnostics, but demands robust processes. In spite of all the advances, isolating, purifying, and interrogating DNA, RNA, exosome/extracellular vesicles (EVs), protein complexes, and other biomarkers directly from biological fluids is still an underdeveloped area [4, 5]. Additionally, we must be concerned with how labile many biomarkers of interest are, as their rapidly degrading, temporal nature necessitates as short as possible a time window between sample collection and isolation/stabilization. Once these biomarkers are safely retained, analysis may begin, leveraging the numerous new analytical technologies under development.

Published in the topical collection *Bioanalytics and Higher Order Electrokinetics* with guest editors Mark A. Hayes and Federica Caselli.

✉ Michael Heller
mheller@ucsd.edu

[1] OHSU Knight Cancer Early Detection Advanced Research Center, 2730 SW Moody Ave, KR-CEDR, Portland, OR 97201, USA

[2] Department of Nanoengineering, UC San Diego, MC 0448, 9500 Gilman Drive, La Jolla, CA 92093-0448, USA

AC electrokinetic methods hold tremendous promise for eliminating the commonly used, slow, and cumbersome centrifugation-based isolation procedures. However, they are generally limited to low conductance conditions (< 0.5 S/m), which now require dilution of the biological sample to reduce its ionic strength. This preprocessing step greatly limits their use for POC devices. DC electrophoretic technologies have been developed for high conductance biological fluids and whole blood processing, but they are largely limited in utility to bulk blood processes and metabolomics. With the exception of Modestino's work developing a thrombin generation assay, which uses a charge separating engineered peptide substrate to monitor thrombin activity, nearly all other technolgies depend on significant sample prep or deproteinization prior to introducing the sample to the device [6]. Nearly all other advancements in whole blood processing in the electrophoretic space are over a decade old. Vrouwe et al., with a chip-based electrophoretic device, were able to successfully determine lithium concentrations from human blood; other papers claiming to work in this same space required substantial sample preparation before assay processing [7, 8].

For low abundance analytes like cell-free DNA/RNA and exosomes/EVs, directly interrogating biological fluids with electric fields is essentially limited to AC dielectrophoretic (DEP) techniques, as DC electrophoresis and electrothermal flow generally lack the specificity needed and electroosmotic forces are swamped out in high conductance media [9, 10]. There is a preponderance of interest in low conductance dielectrophoretic (DEP) technologies, as exemplified by the 443 publications in 2019 alone, according to Google Scholar. Presently, these technologies are still limited in their ability to produce viable sample-to-answer POC devices that are ultimately needed. However, some new AC electrokinetic devices now allow DEP to be carried out under higher conductance conditions [11–15]. Nevertheless, there still remain upper limits to the voltages (~ 15 V) that can be applied to these devices due to electrode damage from the aggressive electrochemistry.

Dielectrophoresis (DEP) is the movement of a particle in a medium as result of an electric field gradient [16]. The DEP force, shown in Eq. 1, can be broken into two major parts: the difference in the complex dielectric properties of a particle and its local medium, and the local electric field gradient near the particle. The magnitude of this effect is scaled by the particle's size and the dielectric properties of the medium.

$$F_{\mathrm{DEP}} = 2\pi\epsilon_m R^3 \left(\frac{\epsilon_p - \epsilon_m}{\epsilon_p + 2\epsilon_m}\right)\left(\nabla E^2\right)$$

The difference in polarizability between the particle and medium, which is a function of frequency, is the keystone that allows for selective manipulation of a target particle range. The particle's relative polarizability is defined by the Clausius-Mossotti relation in Eq. 2, where the real component defines whether the particle will have a translational force up or down the electric field gradient and complex terms describe rotational force effects. It has a real component in the range from − 0.5 to 1; the frequency where CM = 0 is called the crossover frequency.

$$CM = \left(\frac{\epsilon_p - \epsilon_m}{\epsilon_p + 2\epsilon_m}\right)$$

When working in biological media and targeting particulate therein, one does not have control over the dielectric properties of either. Biological particles, running the gamut from extracellular vesicles to intact cells, have exploitable differences in their dielectric properties and dispersion relations, allowing for selectivity through frequency of stimulus. Thus, one must use a combination of electric field control via device geometry and voltage and frequency selection to maximize the desired DEP force and particle selectivity. This optimization ultimately minimizes sample preparation time, and maximizes yield, but must be balanced against device reliability and sample degradation risk. This paper explores the extremes of electric field gradients and frequencies for electrokinetic separations using two different device geometries to determine where limits exist, namely in the form of overheating due to the medium's loss factor and from electrochemical attack of the electrodes themselves.

Materials and methods

Devices

To simulate geometries that might be found in lab-on-a-chip, point-of-care devices, small circular wells were made in polytetrafluoroethylene (PTFE) blocks and spanned by three 100-μm-diameter 99.99% platinum wires (Sigma-Aldrich). A

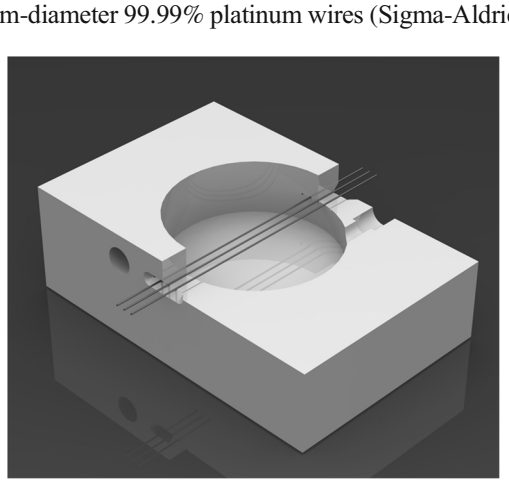

Fig. 1 Rendered cross-section of the wire well device. 3 wires are suspended through the center of the 0.375 in. diameter by 0.1875 in. deep well on 0.015 in. wire-to-wire spacing. The wires themselves are 100 μm in diameter

rendered model of the device is shown in Fig. 1. The diameter of the well is ~ 9.5 mm (0.375 in.) and ~ 4.75 mm deep (0.1875 in.); the wires are spaced on ~ 381 μm center-to-center (0.015 in.) and centered in the middle of the well, both width- and depth-wise. Wires were held under tension and glued in place with cyanoacrylate glue (Scotch single use) and then cured overnight in a 60 °C oven before use. While the ends of the well were firmly affixed, small variations in inter-wire spacing were noted, as result of fabrication imperfections. Devices were cleaned by filling the well with reagent-grade sulfuric acid for 10 min, rinsed thoroughly in 1 MΩ deionized water, and dried in an ~ 60–70 °C oven for at least 30 min before use. Due to the small contact area between the fluid and the glue, minimal chemical attack of the glue was observed. The electrodes are formed by etching a window through a SiO_2 coating to the sputtered Ti-Pt metal layer beneath the oxide. The square grid of these circular electrodes is connected to alternating polarities in a checkerboard pattern, but, in essence, the electrode array is a series interdigitated platinum strip with periodically placed circular windows in the insulation to form the active electrode area. The electrode surface is smooth and bright, with some small grain formation evident at higher magnifications.

Uncoated planar electrode arrays consisting of a checkerboard pattern of 60-μm-diameter circular pads on a 150-μm center-to-center spacing were purchased from Biological Dynamics (La Jolla, CA), and used with no further preparation. The electrodes are formed by etching a window through a SiO_2 coating to the sputtered Ti-Pt metal layer beneath the oxide. The square grid of these circular electrodes is connected to alternating polarities in a checkerboard pattern, but, in essence, the electrode array is a series interdigitated platinum strip with periodically placed circular windows in the insulation to form the active electrode area. The electrode surface is smooth and bright, with some small grain formation evident at higher magnifications. Using COMSOL, Fig. 2 shows the electric field gradients ($\nabla \mid E^2 \mid$) of the respective devices. High field regions remain highly localized to the electrode's outer edges and decrease rapidly as the field extends into the electrolyte, decreasing orders of magnitude within tens of microns of the surface.

The devices were observed under an Olympus BX51WI microscope and Olympus DP71 camera controlled with Olympus's DP Manager software. To power the system, a HP/Agilent 33120 signal generator was connected to an amplifier (Newtons4th LPA01) and, subsequently, to the device under test. All tests used either DC or sinusoid signals. The wire-based device was configured with the inner wire connected to the opposite polarity of the outer wires, and the planar electrodes were powered in a checkerboard polarity pattern. Temperature was not measured nor controlled; during use, the planar device was mounted on a ~ 10 °C/W heatsink without any thermal interface material. Wire-based devices are mounted on a glass substrate, but, given the thickness of the PTFE walls, the majority of the generated heat is assumed to be lost through evaporative cooling and passive convection. Voltage levels between the wire electrodes above and planar electrodes are not directly comparable, as the voltage losses from amplifier to planar electrode surface are substantially higher than along the wire, both from trace resistance and contact resistance within the electrical harness to the chip. Similarly, the different geometries will dramatically change the current pathways and have different abilities to manage heat; consequently, corrosive effects will manifest differently on the respective architectures, even though the electrochemistry remains the same.

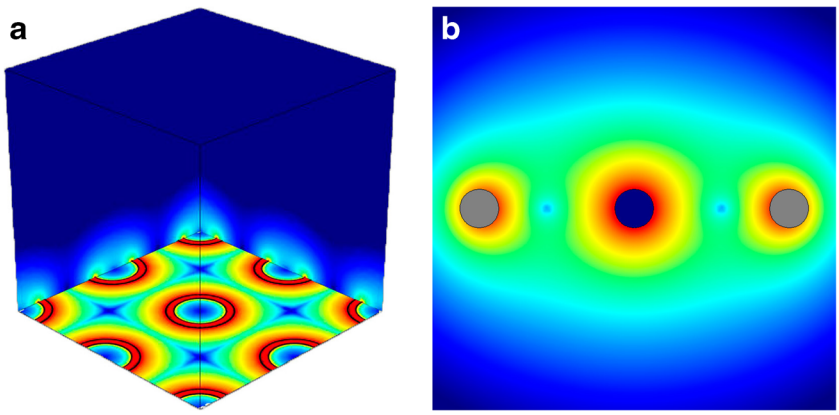

Fig. 2 COMSOL simulations showing the magnitude of the electric field gradient ($\log_{10} \nabla \mid E^2 \mid$) of electrode systems in a 1.4 S/m aqueous electrolyte solution. **a** Is a plot of the planar electrode in 3D; electrodes are powered in a checkerboard pattern, where the electric field gradient is highest around the outer circumference of each electrode, and a null forms in the region between any 4 adjacent electrodes, along with the center of each electrode. **b** The cross-section of a 3-wire suspended electrode arrangement, where the field gradient is symmetric around the center electrode. Low-field gradient regions exist between the electrodes and high field gradients exist at the outer circumference of the wire electrodes. In both cases, high field gradients fall off very quickly, so the bulk solution is $\leq 10^{-6}$ the magnitude of the gradients near the electrodes

A test solution of pH 7.4 10× phosphate-buffered saline (VWR International) is diluted, depending on the test, to either 0.5× or 1× PBS final concentration with 1 MΩ deionized water to roughly simulate the conductivity and salinity of common biological fluids, e.g., blood, plasma, cerebrospinal fluid, and urine. One hundred eighty microliters of solution is needed to fill the wire well devices and 35 μl is needed for the planar electrode devices. After the chambers were filled, respectively, planar and wire devices were stepped through a series of voltages (0–28 V) and frequencies (100 Hz–1 MHz, depending on test) until failure. After voltage and frequency stepping, the parts were flushed with deionized water to remove any precipitated salt and then disassembled. A razor blade was used to carefully separate the glued-on cover of the planar device from the periphery, and then the device was soaked in deionized water before drying in a ~ 60–70 °C oven. The wire-based devices were first immersed in acetone to dissolve the cyanoacrylate glue, whereupon the wires were carefully removed with tweezers. The wires were subsequently rinsed with acetone to remove any residue, then soaked in ethanol and deionized water before drying in a ~ 60–70 °C oven. Scanning electron microscope (SEM) images were taken on a FEI/Philips XL30 ESEM.

Results

Wire electrode devices

The first experiment was examining frequency dependence of electrochemical attack; 1 MHz, 100 kHz, and 10 kHz were chosen, starting at the highest frequency. Voltage was stepped from 4 $V_{peak\text{-}to\text{-}peak}$ (V_{pp}) to 24 V_{pp} in 4 V steps: 3 min on, 2 min off to allow for cool down. The well was flushed with DI water and fresh 0.5x PBS was used after both the 16 V_{pp} steps and the 20 V_{pp} steps as result of evaporative loss during these runs. While no visible pitting on the surface of the wires was observed, bubbling became so severe at 24 V_{pp} that the experiments were terminated before the full 3 minutes expired. The voltage sweeps at 1 MHz and 100 kHz showed no corrosion, but stepping down to 10 kHz resulted in notable etching of the wire surface ~ 1:30 into the 20 V_{pp} set point, so tests were terminated. Corrosion was observed to dramatically decrease with increasing frequency. The Faradaic impedance of a Pt-PBS cell also decreases with frequency, meaning mass transport to/from the electrode-electrolyte interface increases [17, 18]. Experimentally, this resulted in much higher currents, and consequently Joule heating; thus, substantial evaporation and gas evolution were observed.

A second set of experiments was conducted to drive the electrodes into complete failure at 1 kHz or 100 Hz; each voltage point was ramped quickly to its target setting and allowed to remain for 5 minutes or until platinum particles were observed coming off the wires. If no degradation of the wires was observed, voltage was increased and the test was repeated. At failure, wires were removed, and a fresh device was made. Voltage required to induce rapid corrosion was highly variable based on the initial electrode surface and length of tests during voltage stepping (not shown): rougher wires corroded at lower voltage, as would be expected from the greater surface area and small localized peaks, where coordination reactions are favorable. Voltages far above the range used for dielectrophoretic separations (typically 10–15 V_{pp}) were chosen to accelerate corrosion and set an upper bound of device operation, albeit substantial hydrolysis and gas formation between the electrodes were observed above normally used potentials, obviating its use in diagnostics.

Direct observations during failure were impossible as the solution quickly turned dark brown from a mixture of dissolved $PtCl_x/PtO_x$ complexes and platinum nanoparticles. Pt nanoparticles experience positive dielectrophoretic forces at the selected frequencies such that, in lower flow regions near the edges of the well, they form into large, extremely delicate, tendril-like aggregates which nearly bridge the gaps between the wires. These Pt nanoparticle aggregates suffer poor surface adhesion and were largely displaced from the wire surface due to shear forces resulting from electrothermally-derived flow around the wires and from hydrolysis-derived gas byproducts. As expected, due to the rapid growth of surface area, the evolution of gas and corrosion increased over time [19]. Observed, but unintentional, failure of platinum electrode-based devices in other research efforts with human plasma showed similar effects to the electrode systems deliberately tested to failure in 0.5×–1× PBS herein. This suggests the underlying mechanism comes from the common elements of human plasma and PBS buffers, namely high salt concentration, especially from chlorine ions. To examine whether oxygen radicals were actively involved in platinum corrosion, pure water and 30% commercial H_2O_2 (Sigma-Aldrich) were ramped through (0–24 V at 100 Hz and 1 kHz). While significant bubbling was found at test higher voltages with 30% H_2O_2, no observable etching was noted in either buffer.

As seen in Fig. 3, aggregates can be found still loosely attached to the center wire (rightmost wire not shown) after the device was tested at 10 V_{pp}, 100 Hz. Figure 4 shows SEM images of a single Pt wire similarly driven into rapid corrosion at 100 Hz and 10 V_{pp}. The uppermost images from Fig. 4 are from a region outside the submerged well: there are a number of dents and scratches on the surface of the wire from device assembly, but the wire is smooth in unaffected regions. The lower panels show the effects of rapid-onset corrosion due to use with aggregates of platinum nanoparticles covering sections of the wire, while other areas show the underlying wire. Optically, these regions appear black, owing to internal reflections, which scatter and attenuate incident light, similar structures to those seen in deliberate Pt black or platinization depositions [20].

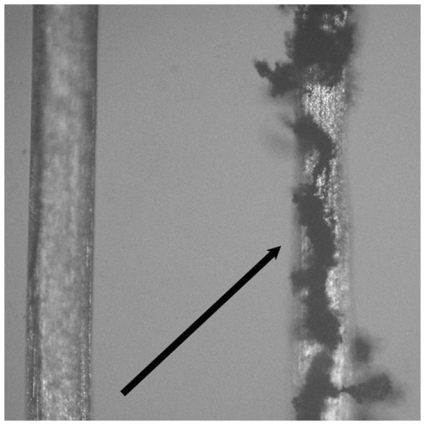

Fig. 3 Left and center wires of a 3-wire device in 1× PBS after application of 100 Hz, 10 V_{pp} for less than 30 s. The black tendril-like aggregates loosely attached to the surface of the central wire are formed from platinum nanoparticles that etched off the surface of the wire (arrow)

The bottom panel of Fig. 4 shows a region with few adhered Pt nanoparticles and, thus, significant striations along the wire axis in the wire beneath are evident. The electric field in the wire electrode geometry is axially uniform over its length; wire resistance (~ 0.4 Ω for a 3-cm-long, 100-μm-diameter wire) and self-inductance (~ 38 nH) are very small compared with the inter-wire impedance, so effectively potential across the wire's length can be assumed to be uniform. Uniform axial striations are consistently observed over the length of the wire. Current density in this configuration is distributed over the length, but skin depth at low frequency (≤ 1 MHz) is much larger than the wire radius. Thus, surface current is almost exclusively radial in nature. It is therefore assumed the striation is due primarily to the grain alignment of the platinum wire and preferential adsorption and reaction kinetics along grain boundaries rather than due to localized current effects.

DC-biased corrosion was also tested on wire electrodes: minimal effects were found at potentials equivalent to damaging AC RMS voltages due to static passivation of the respective surfaces and nonlinear I–V curves. When taken to higher voltages, anodes were driven into rapid corrosion, at rates greater than that found at the same peak-to-peak AC potential. As seen

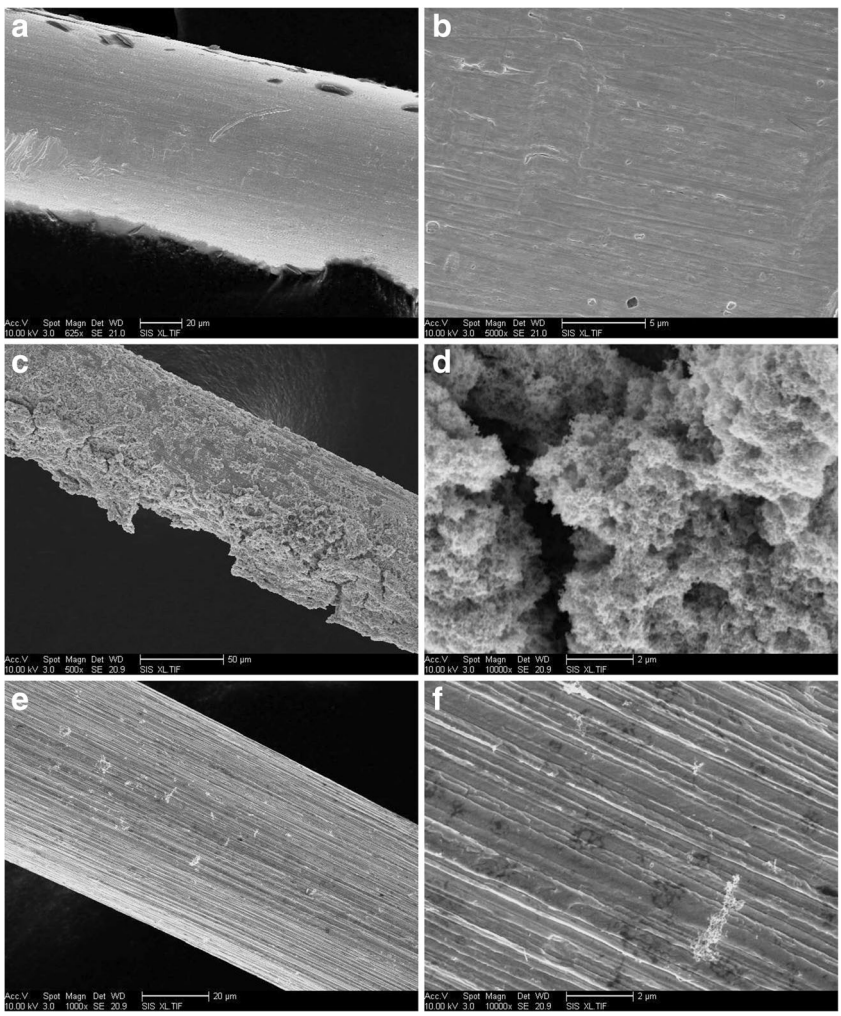

Fig. 4 SEM of a 100-μm Pt wire from the three-wire device comparing a region in air (**a**, **b**) and in submerged/corroded regions (**c**, **d** and **e**, **f**, respectively). Large dark spots are from graphite mounting tape. Given the softness of pure Pt, there are scratches from assembly that show up in the clean section, but the overall surface is largely smooth. The bottom images show adhered Pt nanoparticle aggregates that formed on the wire surface during electrochemical attack from an AC signal (10 V_{pp}, 100 Hz, alternating wire polarity) in 0.5× PBS. While the particles in these images are very small, the size varies significantly over the surface of the wires. Due to the overarching fragility of the aggregated Pt nanoparticle debris, local flow conditions around the wire and subsequent cleaning steps have largely cleaned the underlying Pt wire surface in the bottom two images. The wires appear striated along the primary wire axis, likely due to processes used to initially form the wire. It is undetermined whether these small surface defects were in the as-formed wire, or due to preferential coordination reactions, although the latter is suspected

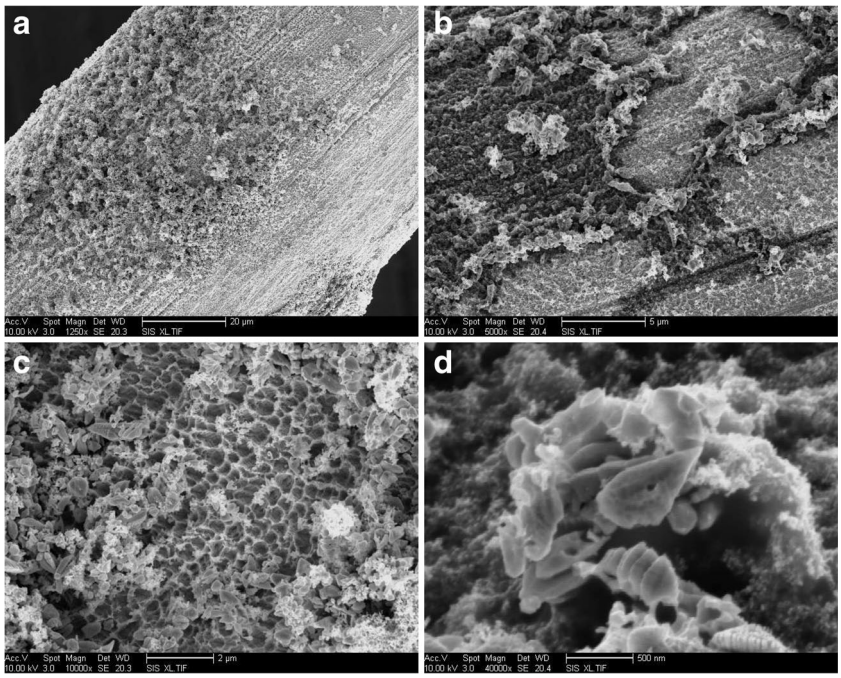

Fig. 5 The center, anode-connected, wire of a wire-based device at 14 V_{DC}, far in excess of that needed to corrode the Pt in 0.5× PBS. Outer wires, connected as cathodes, experienced no surface etching, strongly suggesting the corrosion reactions are chlorine-driven, correlating with data presented by Llopis [23]. Platinum nanoparticle aggregates observed on the corroded surface are similar in morphology and size range to those found on corroded wires held under AC stimulation. Magnification increases from **a** to **d**, showing the morphology in closer detail

in Fig. 5, similar morphology and striations are found on the wire surface for both AC and DC stimulus.

Planar electrode array devices

For planar devices, only low frequency failure modes were examined: sinusoidal drive voltage (1 kHz) was stepped from 10 $V_{peak\text{-}to\text{-}peak}$ (V_{pp}) through 20 V_{pp} in 2 V_{pp}, 5-min steps; and 1.5 V_{pp}, 4.5 V_{pp}, and 10 V_{pp} steps were used at 100 Hz. Figure 6 is a brightfield image of a planar electrode, immersed in 0.5x PBS, tested at 1 kHz, and shown at 16 V_{pp} during its ramp. The left side of Fig. 6 is an unpowered region of the device. Small bubbles formed at the initial 10 V_{pp} stimulus and remained stable until new bubbles began to form at ≥ 18 V_{pp}. At 18 V_{pp}, a few electrodes appear dark in isolated regions, due to roughening of the surface, and the number of darkened electrodes dramatically increases at 20 V_{pp}, becoming largely uniform over the active surface.

Further tests were done on planar electrodes at 100 Hz, stepping from 1.5 V_{pp} to 10 V_{pp}. Low frequency modulation, e.g., 50 Hz or lower, and with DC bias or without, is shown to drastically increase corrosion. Similar effects are not found at higher frequencies due primarily to inherently slow reaction kinetics of Pt/PtOx surface passivation and de-passivation, coupled with reduced ion mass transport to and from the electrode surface [21–23]. While minimal effects were observed at low optical magnification at lower voltages, 10 V_{pp} at 100 Hz resulted in significant bubbling and damage to the electrode surface.

Figure 7 shows the end result of burning out the electrodes at high magnification. The surface first fails at the SiO_2-Pt interface, where the field and current density are highest. Figure 7a and b are from an unused region of the chip for reference. Along the edge of the electrode, larger particles

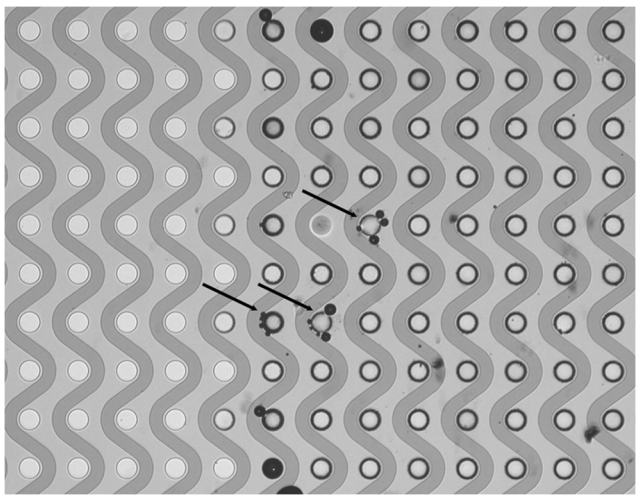

Fig. 6 Brightfield microscope image of a planar electrode immersed in 0.5× PBS during operation at 16 V_{pp} at 1 kHz. The small circles are the active electrode surfaces, and are powered in a checkerboard pattern. For reference, an unpowered region of the planar electrode is shown on the left third where there is no dark outline around the circumference of each respective electrode. A few of the edge electrodes are darker, indicating they have roughened under electrochemical attack. Electrodes were stepped from 14V_{pp} to 20 V_{pp} in 2 V, 5-min intervals. A small amount of bubbling is noted at 14 V_{pp} (arrows), and increases with voltage, as expected from the electrolysis and local boiling. At 18 V_{pp}, electrodes are observed to corrode in localized regions of the chip. By 20 V_{pp}, the extent of the electrode degradation has increased significantly. Drive voltage between wire and planar devices is not directly comparable, but, similarly, lower voltage is needed at 100 Hz to degrade the planar electrodes than at 1 kHz

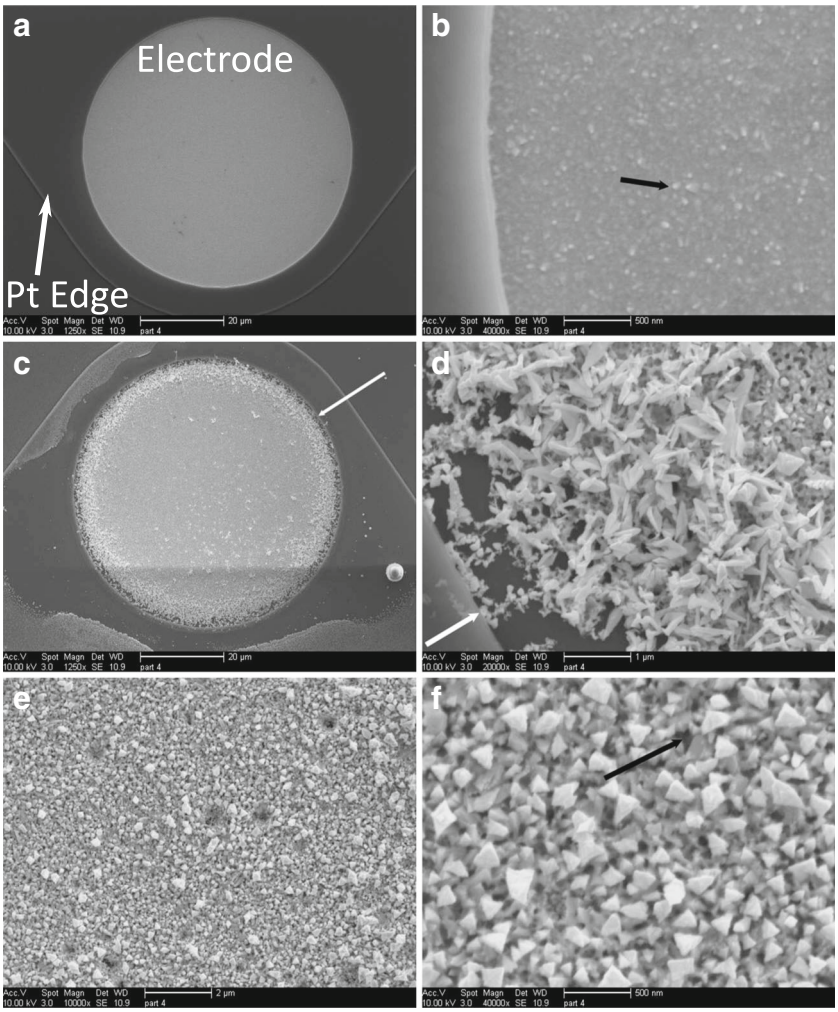

Fig. 7 SEM images of an unused Pt planar electrode. **a** A window in the dielectric-coated surface to underlying Pt trace forms the electrode. The tongue-like lip around the electrode is the edge of the platinum layer. **b** The electrode surface appears continuous and largely smooth with some small grain formation effects due to sputter deposition (arrow). A corroded Pt planar electrode shows a notable difference in the morphology in the center versus at the edges. **c** Electric field, and therefore current, is greatest at the pad-insulator interface (arrow) and relatively uniform over the remainder of the electrode, yielding different local environments. **d** Both the Pt and Ti underlayer are almost completely removed from the Si substrate around the edge, with material piled up along the inward-propagating edge. **e** The center of the electrode has roughened considerably, **f** with a large number of 300–500-nm particles forming on the surface, opening holes to the underlying silicon substrate (arrow to hole)

are observed; as seen in Fig. 7c and d, these particles appear to remain clumped near the receding metallized edge. Due to the higher fields and current density at the outer circumference of the electrode, breakdown occurs there first and then migrates inward. Eventually, the entire electrode roughens and turns visually dark; the reformed surface, cracked and fragmented, remains sufficiently conductive to continue operating in a more limited capacity. The inward migration of particles from the edge is likely due to positive dielectrophoretic force on the recently formed Pt nanoparticles. Electromigration and/or local electrophoresis may possibly contribute to particle movement, but unlikely, given the AC stimulus and particles solely moving towards the center of the electrode [24]. Electromigration may accelerate remodeling of the smooth surface into the granular surface. Throughout the center of the electrode, morphology has fragmented into still-adhered nanoparticles, primarily triangular in shape, and the Si substrate below is visible in the gaps between particles. Figure 7e clearly shows the surface roughening, and Fig. 7f shows the nanoparticle formation in detail.

Similarly interesting is the undercutting of the platinum at the edge of its patterning. As can be seen in Fig. 7c along the upper left edge, there is a significant roughening of the platinum underneath the SiO_2 coating. This suggests that the oxide layer is not completely conformal as it steps from the Si to the Pt layer, allowing for electrolyte ingress and, thus, corrosion at these weak spots. Like wire-based tests, no corrosion was observed in duplicated tests using 1 MΩ deionized water or 30% commercial H_2O_2.

Discussion

Platinum electrodes, when immersed in most aqueous solutions, will produce a stable PtO_x passivation layer, forming the basis for reliable working electrodes for most electrochemical applications. While platinum electrodes are commonly and reliably used for a number of bio-electrical applications, they accumulate damage over their lifetime, even when used at low potentials [25]. High overpotential voltages, under either DC

stimulus or low frequency AC stimulus, in combination with ions that form coordination complexes with surface PtO_x, such as dissolved halogen anions (Cl^-, etc.), will cause the platinum surface to rapidly corrode, ultimately destroying the device. Mechanisms most importantly related to ultimate corrosion of the surface are the reaction kinetics of the PtO_x passivation, and irreversible coordination reactions from strong oxidizers. Voltage plays a double role here, as overpotential will dramatically change the local passivation layer's condition along with the adjacent anion concentration, and drive the magnitude of Joule heating in the system, providing respectively more or less thermal activation energy to these reactions. Mass transport of cations and anions becomes further and further limited with increasing frequency of AC electrical stimulus and, similarly, becomes limited in reaction kinetics by a smaller period of favorable electrode potential.

Prior research into platinum electrode corrosion has typically focused on potentials at or below the reduction potential of water (~ − 1.23 V) in various aqueous acids and at relatively low current densities [18, 21–23, 26–33]. Juchniewicz's results using 3% and 10% NaCl aqueous solutions agreed with tests using HCl solutions [18, 22]. Benke and Gnot further examined dissolution of platinum in HCl, H_2SO_4, and KOH under various conditions and stimulus [34]. Llopis, testing under 4 M HCl and 3 M $HClO_3$ conditions, observed a substantial increase in anodic corrosion above an electrode potential of 1.8 V, attributed to a change in the platinum oxide surface layer [30]. Llopis and Sancho tested Pt corrosion in hydrochloric acid solutions under low frequency AC current stimulus (50 Hz sinusoid, and 10 Hz square wave) and found that corrosion is critically dependent on the removal of surface passivation [23]. Other acids did accelerate corrosion, but generally at a lower rate. Sufficiently, high DC bias relative to AC modulation limits mass transport away from the interface, as does increasing the modulation frequency, at least on a per-cycle basis. Thus, the amount of overpotential tolerated by the electrodes without substantial corrosion increases with frequency, even though it comes with a concomitant increase in Joule heating due to lower effective impedance between the electrodes with the decrease in double-layer capacitance at the interface [35].

Their findings corroborate with those found here: namely, chlorine concentration, temperature, frequency, and current density are the key determinants behind platinum dissolution. The respective device architectures had different inflection points and even the individual devices exhibited enough variability in performance to make the results herein more descriptive of the trends in operating dielectrophoretic devices in high conductance biological fluids than specific guidelines. When working in biological fluids, especially blood products, chlorine concentrations and conductivity are high, accelerating reaction kinetics and further reducing margins of device operation. As noted in results, boiling of the test fluid was observed at high voltages after stepping up from 10 to 100 kHz and 1 MHz. This raises concerns about degradation or denaturation of the sample itself under high temperatures, again limiting upper bounds for voltage. Higher drive voltage directly relates to the electric field gradient, increasing dielectrophoretic forces and, consequently, device selectivity and throughput. Critically speaking, any frequency and voltage choices for corrosion reasons must be balanced in consideration with the target material and system. There is a competition between the optimal frequency window for the dielectrophoretic isolation of small particles from biological solutions (roughly less than 30 kHz), higher frequencies to protect the platinum electrodes, low voltages as to not overheat the media, and high enough dielectrophoretic forces to collect material in a timely fashion. This said, an important conclusion to be drawn is to determine the frequency range of dielectrophoretic isolation for the targeted particle and then operate at the higher end of that frequency range. Reactive oxygen and chlorine species evolving off the electrodes are of concern as well, given their efficacy in degrading biological samples [36]. Evolution rates are drastically lower at current densities typically found in microfluidic systems, but long tests may accumulate to a significant concentration [22]. To date, no studies into oxidative damage in a microfluidic electrokinetic cell have been found, but this does remain a concern.

Possible alternate solutions are the inclusion of a permeable interface layer to the electrode surface and dilution of sample in a nonreactive, low conductance buffer. While acting as an inline impedance, a permeable membrane will materially lower ion flux to/from the platinum surface, greatly limiting chemical attack and acting as a sacrificial layer for reactive oxygen and chlorine species local to the surface. Depending on material selection, the benefit of the additional membrane may offset the loss in electric field. Lastly, the issues of chlorine concentration and conductivity can be greatly mitigated by dilution in low conductivity buffers bereft of reactive metals or halogens [37]. This option has a number of risks involved with its interaction with biological fluids and possible selective loss in yield of targeted particles, even if the same effective amount of biological fluid is exposed to the device. Future dielectrophoretic devices for direct sampling of biological media should pursue smaller feature sizes: scaling geometry down increases field gradients, meaning drive voltage, with its attendant issues, can be decreased. New devices and architectures are ultimately the way forward.

Conclusion

Electrokinetic devices, specifically AC dielectrophoretic separation devices, were tested to failure in blood products and buffers across a range of voltages and frequencies to find the maximum operating space for throughput, and then examined

for root causes. These devices were ultimately limited by electrochemical attack of the platinum electrodes by chlorine at 10 kHz and below. The liquid medium ultimately boiled at higher frequencies and voltages, even though the electrodes remained intact. Unfortunately, high chlorine concentration and overall high conductivity (> 0.5 S/m) is the norm for biological solutions, albeit within typical ranges, so any device designed to operate in this regime must place an emphasis on mitigating corrosion and on electrode design that minimizes voltage requirements. Likewise, frequency choice is one that should be made carefully to balance dielectrophoretic force against electrode and sample damage. Depending on the process, e.g., dielectrophoretic separations of small biological particles and cellular fragments from blood/plasma/serum, the maximum separation peak is fairly broad, allowing one to design a device for higher frequency, where greater system reliability can be found and possibly allow for a wider drive voltage margin, depending on one's design compromises.

Miniaturization and integration of diagnostic devices, as seen in so many other technological fields, must be the driving force towards point-of-care assays. Electrokinetic implementations are a natural fit for this application space, limiting the need for mechanical pumps and greatly simplifying overall workflow complexity. These systems need to integrate directly with biological fluids including blood products, where the effects described in this research will become dominant as productivity and throughput are maximized. The results discussed herein emphasize the need to miniaturize to reduce drive voltage, albeit the sweet spot for frequency and voltage on any specific device will require its own optimization within the bounds explained here.

Funding information This work was funded through MJ Heller's UCSD invention royalties.

Compliance with ethical standards

Conflict of interest Michael Heller is a member of the scientific advisory board for Biological Dynamics. The other authors declare that they have no conflict of interest. This work is based on the thesis of Daniel Heineck, "High-Conductance Electrokinetic Device Characterization and Design" [38].

References

1. Ye S. Evaluating platelet activation related to the degradation of biomaterials using molecular markers. Colloids Surfaces B Biointerfaces. 2019;184:110–5.
2. Nayak S. Point-of-care diagnostics: recent developments in a connected age. Anal Chem. 2017;89(1):102–3.
3. Lewis JM. Detecting cancer biomarkers in blood: challenges for new molecular diagnostic and point-of-care tests using cell-free nucleic acids. Expert Rev Mol Diagn. 1:187–200.
4. Zhou MZMF. Determination of tryptophan, glutathione, and uric acid in human whole blood extract by capillary electrophoresis with a one - step electrochemically reduced graphene oxide modified microelectrode. Chromatographia. 2016;79:911–8.
5. Serru V. Quantification of reduced and oxidized glutathione in whole blood samples by capillary electrophoresis. Clin Chem. 2001;47:1321–4.
6. Modestino A. Thrombin generation assay in untreated whole human blood. Electroph. 2016:2248–56.
7. Vrouwe EX. Direct measurement of lithium in whole blood using microchip capillary electrophoresis with integrated. Electroph. 2004;25:1660–7.
8. Cheng HL. On-line stacking capillary electrophoresis for analysis of methotrexate and its eight metabolites in whole blood. Electroph. 2008;29:3665–73.
9. Lewis JM. Integrated analysis of exosomal protein biomarkers on alternating current electrokinetic chips enables rapid detection of pancreatic cancer in patient blood. ACS Nano. 2018;12:3311–20.
10. Mohammadi M. Hydrodynamic and direct-current insulator-based dielectrophoresis (H-DC-iDEP) microfluidic blood plasma separation. Anal Bioanal Chem. 2015;407:4733–44.
11. Ibsen S. Recovery of drug delivery nanoparticles from human plasma using an electrokinetic platform technology. Small. 11:5088–96.
12. Ibsen SD. Rapid isolation and detection of exosomes and associated biomarkers from plasma. ACS Nano. 2017;11(7):6641–51.
13. Manouchehri S. Dielectrophoretic recovery of DNA from plasma for the identification of chronic lymphocytic leukemia point mutations. Int J Hematol Oncol. 2015;5:27–35.
14. Sonnenberg A. Dielectrophoretic isolation and detection of cancer-related circulating cell-free DNA biomarkers from blood and plasma. Electrophoresis. 2014;35:1828–36.
15. Lewis J. A pilot proof-of-principle analysis demonstrating dielectrophoresis (DEP) as a glioblastoma biomarker platform. Sci Rep. 2019;9:1–10.
16. Pethig R. Dielectrophoresis: status of the theory, technology, and applications. Biomicrofluidics. 2010;4:228–11.
17. Wei XF. Impedance characteristics of deep brain stimulation electrodes in vitro and in vivo. J Neural Eng. 2009;6:30–46.
18. Juchniewicz R. The influence of increasing superimposed 50 c/s a.c. on the anodic dissolution of platinum in 3% sodium chloride. Cor Sci. 1966;6:69–77.
19. Hayes M. Aggregation effects on the electrocatalytic activity of platinum. Acc Chem Rev. 2013;53:88–95.
20. Stanca SE. Chemical and electrochemical synthesis of platinum black. Sci Rep. 2017;7:1–8.
21. Briner E. Recherches sur lectrolyse avec courant ondulé. Observations sur attaque des électrodes de platine et la formation de ozone sous effet du courant alternatif et du courant. Helvetica. 1944;26:1829–35.
22. Juchniewicz R. The influence of alternating current on the anodic behaviour of platinum. Plat Met Rev. 1962;6:100–5.
23. Llopis J. Electrochemical corrosion of platinum in hydrochloric acid solutions. ECS. 1961;108:720.
24. Pyell U. Characterization of nanoparticles by capillry electromigration separation techniques. Electrophoresis. 2010;31:814–31.
25. Wissel K. Platinum corrosion products from electrode contacts of human cochlear implants induce cell death in cell culture models. PLoS One. 2018;13:1–20.
26. Rand DAJ. A study of the dissolution of platinum, palladium, rhodium and gold electrodes in 1M sulphuric acid by cyclic voltammetry. J Elect Chem Int Elect. 1972;35(1):209–18.
27. Kuhn AT. The behaviour of platinum, iridium and ruthenium electrodes in strong chloride solutions. J Elect Chem Int Elech. 1973;41:329–49.

28. Brown SA. Electrochemical corrosion in saline and serum. J Biomed Mater Res. 1980;14:173–5.
29. Black RC. Dissolution of smooth platinum electrodes in biological fluids. Appl Neurophys. 1980;42:366–74.
30. Llopis J. Corrosion of platinum metals and chemisorption. Cat Rev. 1968;2:161–220.
31. Bentley R. The alternating current electrolysis of concentrated acids. J Appl Chem. 2007;7:619–26.
32. Pourbaix MJN. Electrochemical properties of the platinum metals. Plat Met Rev. 1959;3:47–53.
33. Llopis J. Study of the impedance of a platinum electrode in the system. Electro Acta. 1959;8:130–50.
34. Benke G. The electrochemical dissolution of platinum. Hydrometallurgy. 2002;64:205–18.
35. Franks W. Impedance characterization and modeling of electrodes for biomedical applications. Trans biomed Eng. 2005;52:1295–302.
36. Czarnetzki LR. Formation of hypochlorite, chlorate and oxygen during NaCl electrolysis from alkaline solutions at an RuO_2/TiO_2 anode. J App Elect. 1992;22:315–24.
37. Cherevko S. A comparative study on gold and platinum dissolution in acidic and alkaline media. J Electrochem Soc. 2014:161–82.
38. Heineck DP. High-conductance electrokinetic device characterization and design. University of California San Diego. 2017. https://escholarship.org/uc/item/0xp4r2hb. Accessed 28 Feb 2020.